Supporting Information

Shain et al. 10.1073/pnas.1114817109

SI Text

Characteristics of SWI/SNF Mutations. From the study by Jones et al. (1) of full exomic sequences from 24 pancreatic cancer cases, mutation types breakdown as follows: synonymous (25.5%), missense (62.4%), nonsense (3.8%), indel (5%), and splice-site/UTR (3.3%). Of the nine point mutations hitting components of the SWI/SNF complex (summarized in Table 1), there were no synonymous mutations but seven nonsense, indel, or splice-site mutations, indicating a skew toward functionally relevant mutations. Three of these mutations were also associated with loss of heterozygosity, a classic tumor suppressor pattern. In addition, of the 20,661 genes sequenced in that study, only 148 showed two or more mutations (among the 24 samples). Notably, 3 of those 148 genes encode subunits of the SWI/SNF complex.

Determining SWI/SNF Inactivation Frequency. For this analysis (summarized in Table S1), we combined our high-resolution array CGH data of 70 pancreatic cancer samples, along with the SNP array data of 7 additional samples from the Wellcome Trust Sanger Institute's CONAN database (2). Homozygous deletions were called for samples with $\log_2$ ratios of −2 or less. Focal heterozygous deletions were defined as deletions (circular binary segmentation $\log_2$ ratio values less than −0.2) that spanned no more than five genes (in addition to the presumptive SWI/SNF target). For mutations, we restricted our analysis to the sequencing data reported by Jones et al. (1), which represented the only unbiased whole-exome screen.

Of the four types of alterations (tabulated in Table S1), each is mutually exclusive except potentially heterozygous deletions and homozygous mutations, the latter of which may reflect mutation plus deletion. In our analysis, the two genes with focal heterozygous deletions did not have reported mutations. Moreover, in the datasets analyzed here, there was only one instance of a sample (PANC1) having a focal aberration in two different SWI/SNF components. Thus, we are unlikely to be overestimating the reported frequency (34%).

Indeed, the loss of SWI/SNF components is more likely being under-called. For example, we did not count any of the numerous semifocal deletions (<1.5 Mb) targeting *ARID1A* (Fig. 1*C*). We also did not include any of the broader losses (e.g., whole-chromosome arms) that span SWI/SNF genes. Thus, our estimate that a component of the SWI/SNF complex is lost in 34% of tumors is likely a conservative underestimation of the true frequency.

1. Jones S, et al. (2008) Core signaling pathways in human pancreatic cancers revealed by global genomic analyses. *Science* 321:1801–1806.

2. Bignell GR, et al. (2010) Signatures of mutation and selection in the cancer genome. *Nature* 463:893–898.

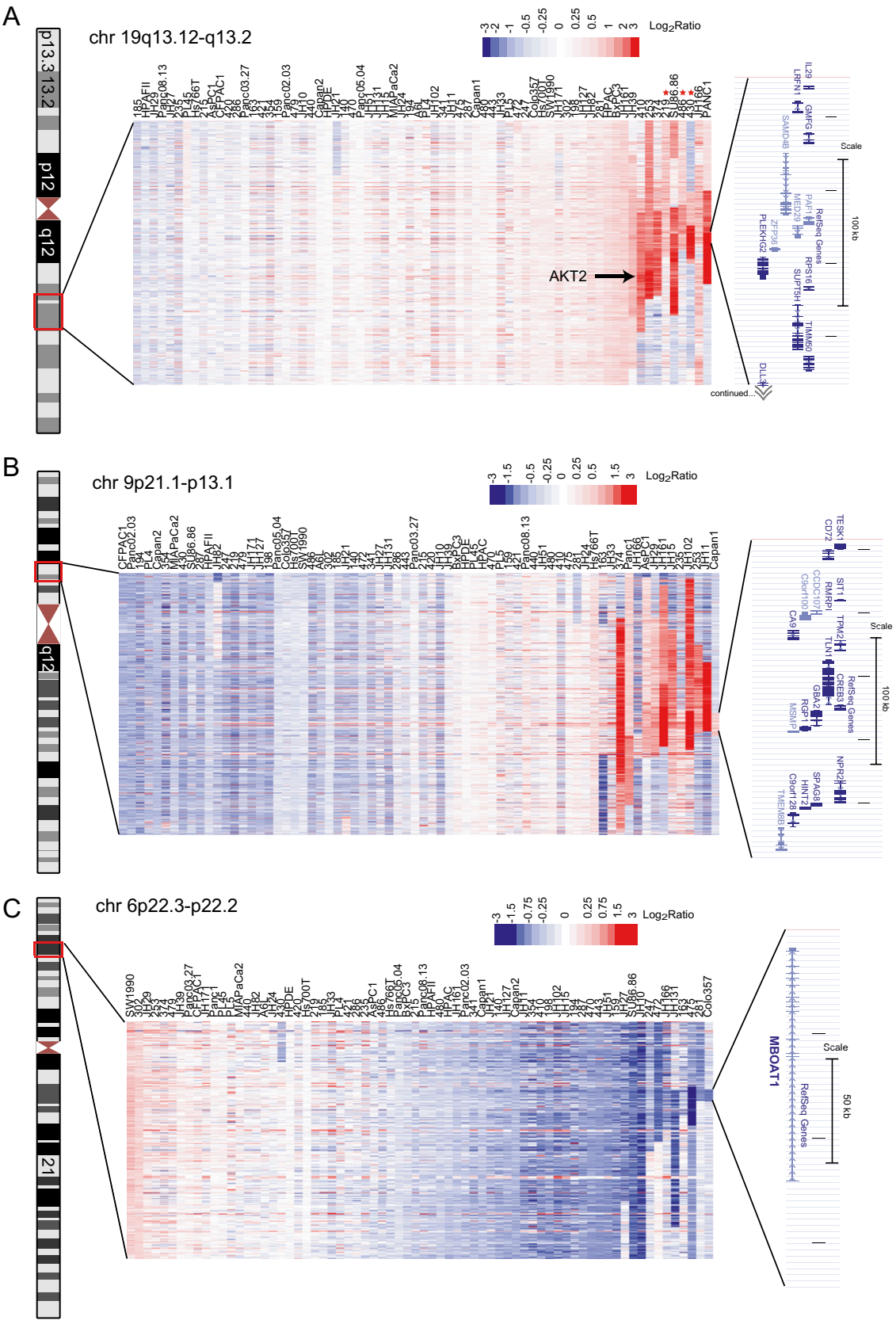

Fig. S1. Newly identified DNA copy number alterations in pancreatic cancer. The heat maps depict gains (red) and losses (blue) at select recurrently altered loci. (*A*) Recurrent amplification within 19q13.2, proximal to *AKT2*. Samples denoted by star exclude *AKT2*. (*B*) Recurrent amplification within 9p13.3. (*C*) Recurrent deletion within 6p22.3 targets *MBOAT1*, encoding a presumptive membrane-bound O-acetyltransferase.

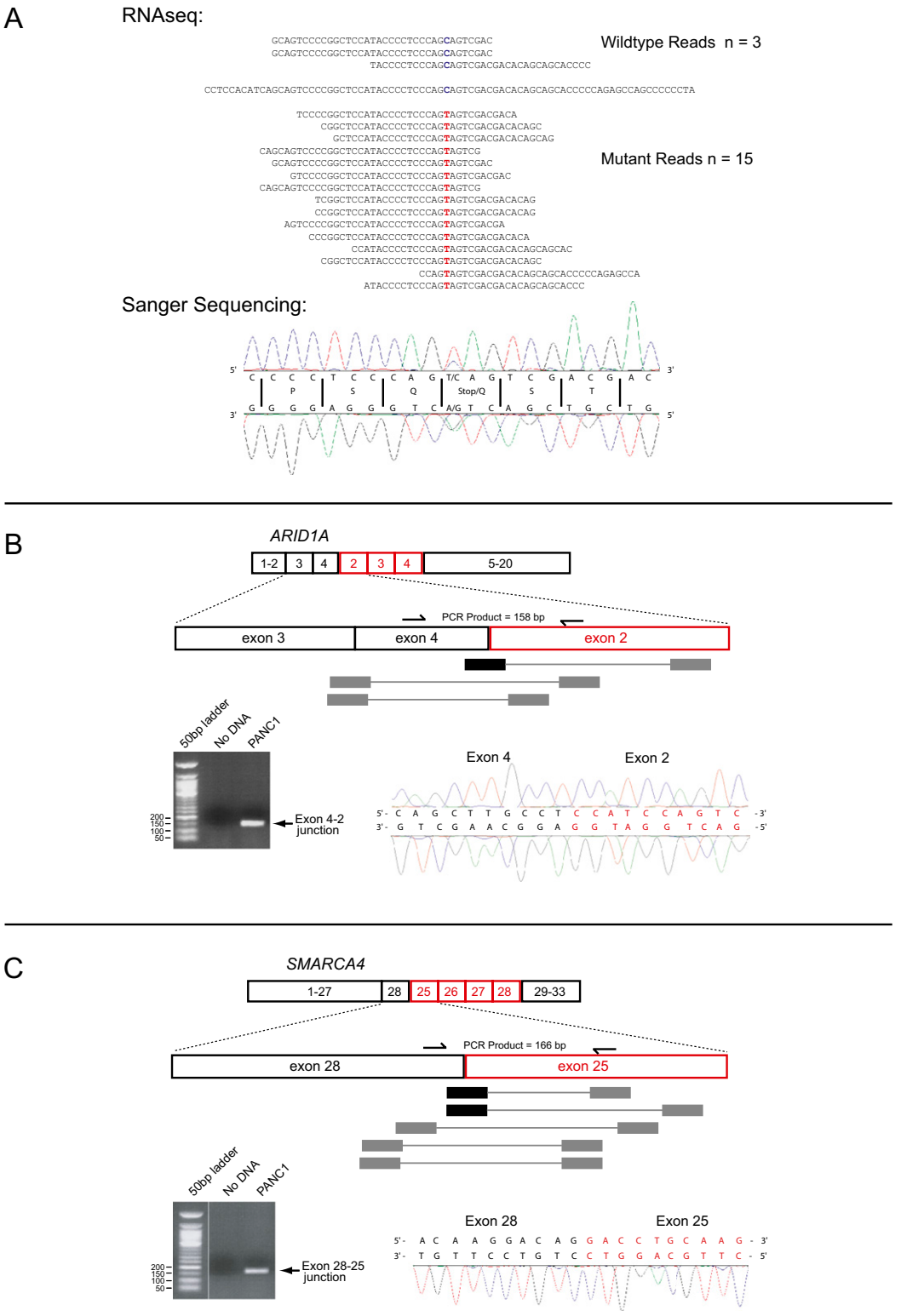

Fig. S2. Transcriptome sequencing identifies additional SWI/SNF subunit aberrations. (*A*) (*Upper*) Paired-end RNAseq reveals *ARID1A* exon 3 nonsense mutation (Q538X) in Hs766T cells. WT and mutant reads are shown aligned to the reference sequence. (*Lower*) Mutation is validated by Sanger sequencing of PCR-amplified DNA. Note that despite the mutation being heterozygous, a low fraction of WT reads (17%) suggests the possibility of epigenetic silencing of the WT allele and is consistent with a lack of observed protein (Fig. 3). (*B*) Paired-end RNAseq identifies a rearrangement of *ARID1A* in PANC1 cells, consistent with an in-frame internal duplication of exons 2–4. (*Upper*) Shown is a schematic depiction of the predicted transcript structure, supported by paired-end reads (black rectangle represents a chimeric read spanning the newly identified exon junction). (*Lower*) Rearranged exon structure is confirmed by PCR amplification and sequencing across the exon junction (PCR product and Sanger sequence are shown). (*C*) Paired-end RNAseq reveals a rearrangement of *SMARCA4* in PANC1 cells, consistent with a frame-shifting internal duplication of exons 25–28. The rearrangement is schematically depicted and validated as above.

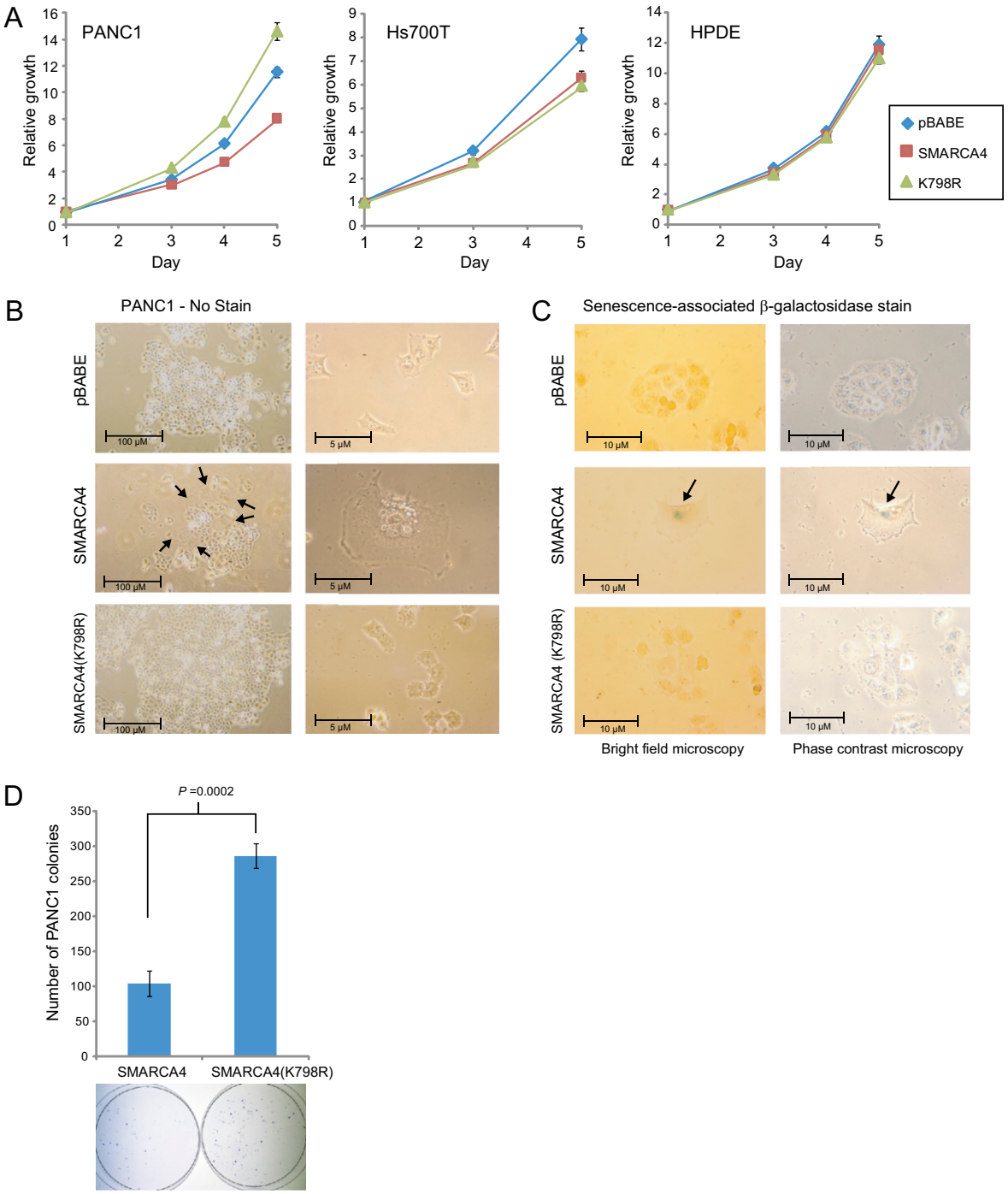

Fig. S3. Further characterization of SMARCA4 re-expression in pancreatic cell lines. (*A*) Complete time course depicting growth of HPDE, PANC1, and Hs700T cells, each stably transduced with empty vector (pBABE), SMARCA4, or SMARCA4 (K798R). (*B*) Photomicrographs of PANC1 cells stably transduced with empty vector, SMARCA4, or SMARCA4(K798R) show a distinctly enlarged, flattened morphology selectively in SMARCA4-expressing cells. Representative low- and high-magnification fields are shown. The arrows denote representative cells exhibiting the altered morphology. (*C*) Representative photomicrographs (bright field and phase contrast) of PANC1 stable transductants stained for senescence-associated β-galactosidase (blue stain, arrows). (*D*) Transfection of SMARCA4 into PANC1 cells (deficient of SMARCA4) reduces clonogenic efficiency (colony growth on plastic) compared with enzymatically inactive SMARCA4 (K798R) mutant.

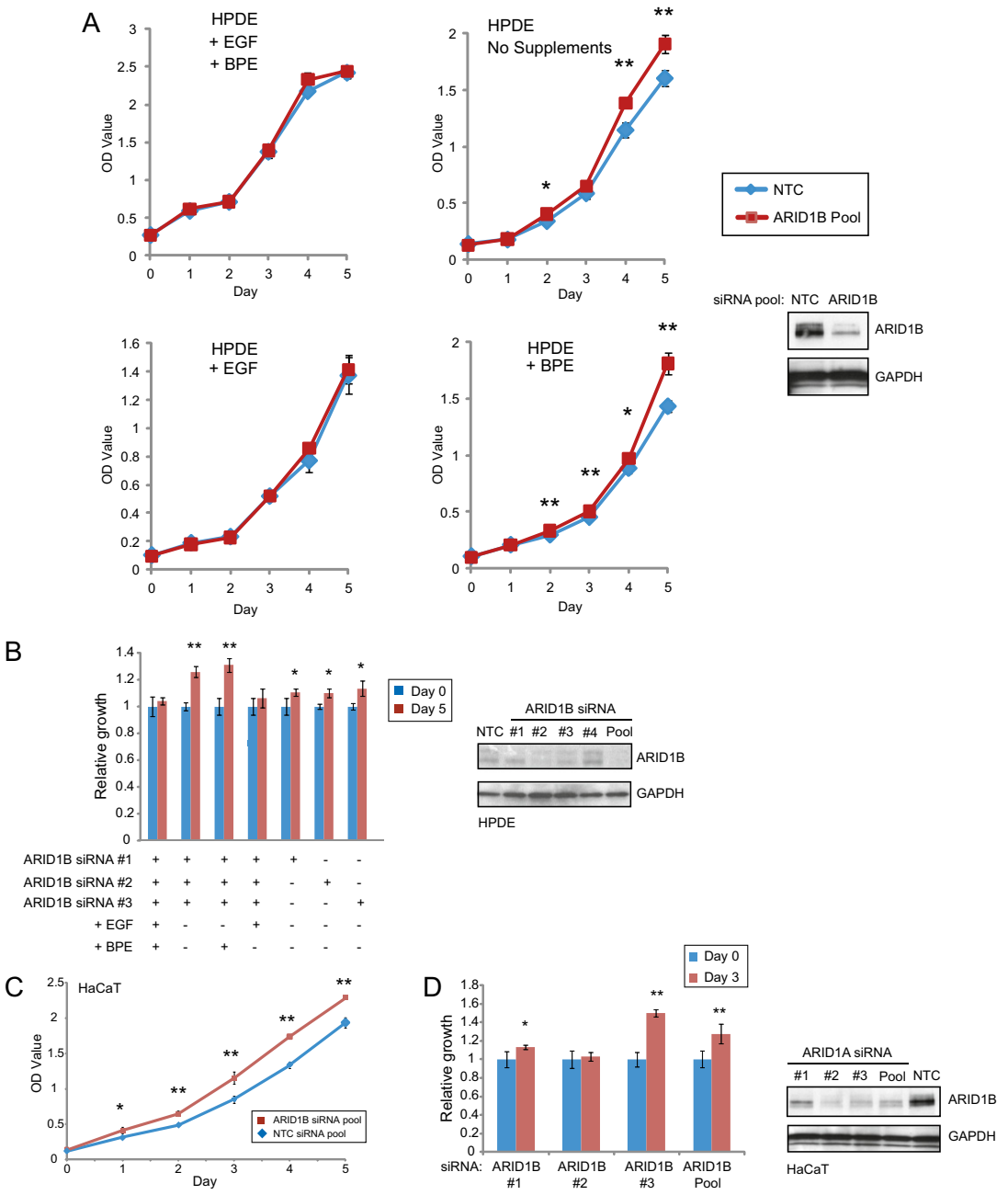

Fig. S4. Characterization of ARID1B knockdown-associated growth-enhancing phenotypes. (*A*) (*Left*) Time courses of cell growth (measured by WST-1 assay) comparing siRNA pools targeting ARID1B (red) and nontargeting control (blue) in the presence or absence of EGF and bovine pituitary extract (BPE). **P* < 0.05; ***P* < 0.01 (pairwise comparisons, Student *t* test). (*Right*) Western blot verifies ARID1B knockdown. Note that ARID1B knockdown enhances cell growth in the absence of EGF. (*B*) (*Left*) Bar graph depicts ratios of cell growth of HPDE cells transfected with individual or pooled siRNAs targeting ARID1B compared with nontargeting control, in the presence or absence of EGF and BPE, and assayed at day 0 (blue bars) and day 5 (red bars); day 0 ARID1B-targeted/control cell growth is set to 1. *P* values are indicated as above. (*Right*) Western blot verifies ARID1B knockdown by individual and pooled siRNAs. That different individual siRNAs targeting ARID1B confer the same enhanced EGF-independent growth phenotype effectively excludes an off-target RNAi effect. (*C*) ARID1B knockdown enhances growth of HaCaT cells. *P* values are indicated as above. (*D*) (*Left*) Bar graph depicts ratios of cell growth of HaCaT cells transfected with individual or pooled siRNAs targeting ARID1B compared with nontargeting control, in complete media [DMEM + 10% (vol/vol) FBS], and assayed at day 0 (blue bars) and day 3 (red bars); day 0 ARID1B-targeted/control growth is set to 1. *P* values are indicated as above. (*Right*) Western blot verifies ARID1B knockdown by individual and pooled siRNAs. That different individual siRNAs targeting ARID1B confer the same growth enhancement excludes an off-target RNAi effect.

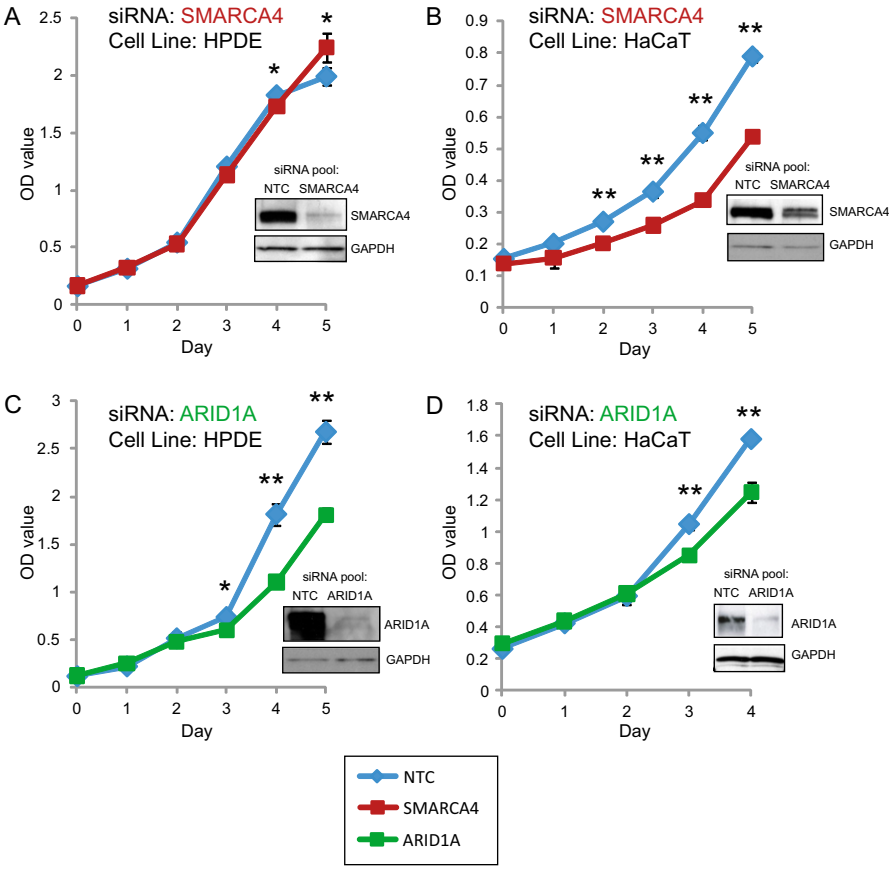

Fig. S5. SMARCA4 and ARID1A knockdown phenotypes in HPDE and HaCaT cells. Panels display time courses of cell growth, quantified by WST-1 assay. HPDE and HaCaT cells were transfected with siRNA pools targeting SMARCA4 or ARID1A, compared with the nontargeting control (NTC) siRNA pool. Western blots confirming knockdown are shown for each panel. *$P < 0.05$; **$P < 0.01$ (pairwise comparisons, Student *t* test). (*A*) SMARCA4 knockdown has a nominal effect on growth of HPDE cells. (*B*) SMARCA4 knockdown reduces growth of HaCaT cells. (C) ARID1A knockdown reduces growth of HPDE cells. (*D*) ARID1A knockdown reduces growth of HaCaT cells. Note the distinct kinetics of ARID1A knockdown-associated growth reduction, where the effect only becomes apparent on day 3.

Table S1. Frequencies of SWI/SNF subunit aberration in pancreatic cancer

Gene	Homozygous deletion	Focal heterozygous deletion	Homozygous mutation	Heterozygous mutation	Focal aberration frequency, %
SMARCA2	1	1	0	0	2.59
SMARCA4	1	0	1	1	9.63
ARID1A	0	0	0	2	8.33
ARID1B	2	1	0	0	3.89
PBRM1	1	0	1	1	9.63
Sum	5	2	2	4	34.1
Samples, *n*	77	77	24	24	

Table S2. SWI/SNF components mutated in ovarian clear cell carcinoma

Gene name (transcript accession identification)	Tumor	Amino acid	Mutation type	Frequency
ARID1A (CCDS285.1)	OCC01PT	fs	Indel	62% (5 of 8)
	OCC02PT	p.Q185X	Nonsense	
	OCC02PT	fs	Indel	
	OCC03PT	fs	Indel	
	OCC07PT	p.Y195X	Nonsense	
	OCC08PT	fs	Indel	
ARID1B (CCDS5251.1)	OCC02PT	fs	Indel	12.5% (1 of 8)
SMARCA4 (CCDS12253.1)	OCC06PT	p.F1102L	Missense	12.5% (1 of 8)